Adriano Henrique[1,2,3]
Mohsen Karimi[1,2,3,*]
José A.C. Silva[2,3]
Alírio E. Rodrigues[1]

Analyses of Adsorption Behavior of CO_2, CH_4, and N_2 on Different Types of BETA Zeolites

The adsorption equilibrium and kinetics of CO_2, CH_4, and N_2 on three types of BETA zeolites were investigated at different temperatures and a defined partial pressure range from dynamic breakthrough experiments. The adsorbed amount followed the decreasing order of $CO_2 > CH_4 > N_2$ for all studied materials. For the same ratio of SiO_2/Al_2O_3, the Na-BETA-25 zeolite showed a higher uptake capacity than H-BETA-25, due to the presence of a Na^+ cationic center. Comparing the same H^+ compensation cation, zeolite H-BETA-25 expressed a slightly higher adsorption capacity than H-BETA-150. Regarding the selectivity of gases, based on their affinity constants, H-BETA-150 displayed the best ability. The adsorption kinetics was considered using the zero-length-column (ZLC) technique. Response surface methodology (RSM) was applied to evaluate the interactions between adsorption parameters and to describe the process.

Keywords: Adsorption equilibrium, Natural gas upgrading, Response surface methodology, Zeolite BETA, Zero-length-column technique

Received: July 26, 2018; *revised:* September 24, 2018; *accepted:* November 20, 2018

DOI: 10.1002/ceat.201800386

Supporting Information available online

1 Introduction

1.1 Biogas Upgrading and Natural Gas Purification

The separation and purification of industrial commodities, e.g., gases, fine chemicals, and fresh water, are conjoined with high-energy-cost projects (15 % of global energy production) and the demands of such products are estimated to have a triple rise by 2050 [1]. While carbon dioxide (CO_2) has a stronger effect than other gases on energy fields to implement successful separation and purification technologies, it is also one of the main causes of climate change. So, carbon capture and storage (CCS) is a vital step in different processes including natural gas sweetening, biogas upgrading, landfill gas purification, and also post-combustion processes [2–5].

Among all of these technologies, biogas has a significant importance as a promising renewable energy source and is characterized by economical costs. While the composition of biogas depends on the sludge and the operation conditions of the digestion process, CH_4 and CO_2 are two main parts of biogas. It also contains some other contaminations (less than 4 %) including N_2, H_2O, H_2S, NH_3, O_2, and siloxane [6]. Thus, in the way of biogas upgrading, these contaminants should be eliminated for applications as a high-quality fuel and a promising replacement for fossil fuels [7]. Among all of the pollutants of biogas, CO_2 is the major one, and the costs of its removal is a most critical step in the upgrading process (CO_2 content less than 3 vol %) [8].

On the other hand, while natural gas is one of the favorable energy sources in the world, the applications of this energy source has still some problems because of the presence of several impurities such as nitrogen and CO_2 [5, 9]. Beside of its toxic effects, CO_2 corrodes the transportation and storage systems in the presence of water. Also, the significant amounts of nitrogen in the natural gas should be purified to meet the pipeline quality for minimum heating value specifications, typically > 90 % methane [9, 10]. As a result, the natural gas upgrading should be implemented during the sweeting processes to meet the "pipeline-quality" methane.

[1]Adriano Henrique, Dr. Mohsen Karimi, Prof. José A.C. Silva, Prof. Alírio E. Rodrigues
mohsen.karimi@fe.up.pt
University of Porto, Laboratory of Separation and Reaction Engineering (LSRE), Associate Laboratory LSRE/LCM, Department of Chemical Engineering, Faculty of Engineering, Rua Dr. Roberto Frias, 4099-002 Porto, Portugal.

[2]Adriano Henrique, Dr. Mohsen Karimi, Prof. José A.C. Silva
Instituto Politécnico de Bragança, Laboratory of Separation and Reaction Engineering (LSRE), Associate Laboratory LSRE/LCM, Department of Chemical and Biological Technology, Campus de Santa Apolonia, 5300-857 Braganca, Portugal.

[3]Adriano Henrique, Dr. Mohsen Karimi, Prof. José A.C. Silva
Grupo de Processos e Produtos Sustentáveis, Centro de Investigação de Montanha (CIMO), Campus de Santa Apolonia, 5300-253 Braganca, Portugal.

1.2 Purification and Upgrading Techniques

Biogas upgrading in methane is a requisite step for its applications as a vehicle fuel, industrial usages, and in the national grids, which is primarily achieved by CO_2 and nitrogen elimination [11]. Currently, several methods are in use on the commercial scale for biogas upgrading to meet '"pipeline-quality" criteria. These techniques are categorized as physical (e.g., pressure swing adsorption) [12, 13], chemical (e.g., amine scrubbing) [14], membrane-based process [15], cryogenic process [16], and chemical conversion [17].

Among these methods, adsorption processes by solid porous crystalline materials due to the environmental criteria and lower capital costs have become an increasingly competitive and favorable strategy for small- to medium-scale operations. Also, studies are ongoing to achieve the industrial scale [18]. In this process, a component in the gas stream due to the physical or van der Waals forces transfers to the surface of solid porous materials, then it is trapped by the available cavities. Gas sequestration by physical adsorption is employed by various solid adsorbents, including porous carbons [19], metal organic framework materials [20–23], zeolites [24, 25], lithium zirconate [26], and silicon-based mesoporous materials [27]. Among the most favorable ones are zeolites due to their high uptake capacity, low preparation cost, and easy synthesis.

1.3 Zeolites

Zeolites are microporous crystalline aluminosilicates and have a well-defined 3D framework structure with a TO_4 (T is normally Si or Al) tetrahedral corner, by sharing a basic building unit. These tetrahedral basic units can form moieties with 6-rings, 8-rings or even 12-rings [28, 29]. Considering the regeneration conditions of zeolites after several usages, their abilities for liquid and gaseous media, and also their unique molecular sieving properties, these adsorbents are among the most promising ones [30]. Moreover, compensation of aluminum atoms which are present inside the zeolite framework with exchangeable cations (often alkali cations) in the pore space gives structurally tuned zeolites, and enables them to adsorb a wide range of gas molecules, including CO_2, CH_4, and N_2.

According to the International Zeolite Association (IZA), more than 250 unique zeolites topologies are reported [31]. Here, BETA zeolite has been considered as adsorbent material because of its superior structural features. This adsorbent was first synthesized by Wadlinger et al. [32], using tetraethylammonium cation (TEA) as an organic structure, directing agent (SDA) at the mobile research and development laboratories. After that, the structural determination of BETA zeolite was presented for the first time by Treacy and Newsam [33]. Based on their study, BETA has a very open crystalline structure with high surface area and consists of 3D interconnected large pores, with both sinusoidal and linear channels (diameters of 0.55×0.55 nm and 0.76×0.64 nm, respectively) [33].

Also, ion-exchange capacities and abilities should be synthesized at a wide chemical composition, i.e., SiO_2/Al_2O_3 ratios [33–35]. This quality makes it a valuable candidate for CO_2 adsorption because of the control of this molar ratio by adjusting the number of acid sites and the hydrophilic/hydrophobic character of this adsorbent. These combined superior characteristics introduce BETA zeolite as an admissible material for different applications in the petrochemical and fine chemistry, biomass and environmental chemistry [36].

In the literature, there are only a few studies on CO_2 selectivity over other gases regarding equilibrium separation using zeolite BETA [37–41]. First, Xu et al. [37] studied the adsorption of CO_2, CH_4, and N_2 on BETA zeolite by the exchange of compensation cations (H^+ and Na^+ forms) at 273 K and 303 K and also at 0–1 bar, by employing a static volumetric system. They showed that the Na^+ form contributes to higher adsorbed amounts than the H^+ form for all considered gases. They also studied the adsorption of CO_2, CH_4, and N_2 on the BETA zeolite with monoethanol amine (MEA, 40 wt %) incorporated framework (MEA(40)-β) at 303 K and 1 bar. They observed that the CO_2/CH_4, CO_2/N_2, and CH_4/N_2 selectivities were much better than for BETA zeolite without MEA [38].

Also, Huang et al. [39] considered the adsorption equilibrium of CO_2 and CH_4 under high pressure of up to 20 bar at different temperatures (308.1, 318.1, and 328.1 K) by a static volumetric apparatus on the zeolite BETA and found that it had a much higher preferential adsorption for CO_2 than for CH_4. In addition, Yang et al. [38] reported the adsorption behavior of CO_2 on BETA zeolites, which were compensated with different earth metal cations (alkali and alkaline), in series. The adsorption capacity of CO_2 decreased in the order of $K^+ > Na^+ > Li^+ > Ba^{2+} > Ca^{2+} = Cs^+ > Mg^{2+}$.

On the other hand, BETA zeolite is a strong and robust adsorbent which is widely used in catalysis. One of the main features of BETA zeolite is its ability to be synthesized in a completely de-aluminated form, which improves its hydrophobicity character to the same order of activated carbons [40]. In this way, in the industries of natural gas sweeting and biogas upgrading to separate $CO_2/N_2/CH_4$, which contained a percentage of water, it can be a favorable adsorbent. Thus, in this study, the adsorption of $CO_2/CH_4/N_2$ at different Si/Al ratios and cations was investigated, and it was proved that this adsorbent has reasonable sorption capacity even when the Si/Al ratio changes. This means that apart from having lower adsorption capacities for CO_2 relatively to highly hydrophilic zeolites, such as zeolites 4A, 5A, and 13X, the capability of BETA zeolite to be completely de-aluminated is beneficial for such processes.

1.4 Kinetic Measurement

An adsorption process includes one or more than one adsorbate which is fixed through physical or chemical bonds onto an adsorbent [43, 44]. This process as an efficient and environmentally friendly technique has attracted much attention in the wastewater treatment process [45, 46], and gas separation and purification [47–50], to remove impurities from water or gas. In this way, it is required to develop the adsorption kinetics to evaluate the predicted adsorption parameters with experimental adsorbent values. Regarding the adsorption kinetics, there are several techniques including batch, shallow-bed or single-particle methods and zero-length column (ZLC) to determine

the kinetics parameters [51]. In this study, the ZLC technique was employed as an easy and fast experimental method for kinetics measurement. The ZLC is a differential bed of particles (adsorbents) which is primarily saturated and provides reliable results [52].

1.5 Objectives

A series of breakthrough experiments in a fixed bed were performed to study the dynamics of CO_2, CH_4, and N_2 in three types of commercial BETA zeolite samples, namely, H-BETA-25, H-BETA-150, and Na-BETA-25. The isotherms were collected from the breakthrough data, and the evaluation of adsorption values was performed by the Langmuir model to determine the adsorption parameters including equilibrium constants, heat of adsorption, Henry's constants, and saturation capacities. Adsorption kinetics was also studied on all BETA zeolites for CO_2 adsorbate by the ZLC technique. Finally, the response surface methodology (RSM) was applied by using a second-order equation to describe the behavior of the adsorption process and to investigate interactions of the main parameters.

2 Materials and Methods

2.1 Materials

All BETA zeolites were provided by the German company Süd-Chemie, currently acquired by Clariant International Ltd. The supplied materials were characterized by the SiO_2/Al_2O_3 ratio (H-BETA-25, H-BETA-150) and/or compensation cations (Na-BETA-25). In addition, the utilized gases including CO_2, CH_4, and N_2 as adsorbate and He as inert gas were supplied by Air Liquide, in the following purities: CO_2 N48 (99.998 %), methane N35 (99.95 %), nitrogen N50 (99.999 %), and helium ALPHAGAZ 2 (99.9998 %). The physical properties of these gases are reported in Tab. 1.

2.2 Zeolite BETA Samples

H-BETA-25 and H-BETA-150 were in the pellet form, with approximately 20 % of binder, while Na-BETA-25 was in powder form and was transformed to the small agglomerates for fixed-bed adsorption. In this way, the powder materials were compressed into tablets by means of an infrared tablet press machine (under 2 t for 5 min), then they were divided to small agglomerates and sieved. More details about this procedure are reported in the Sect. S1 of the Supporting Information.

2.3 Physical Characterization

The characterization of adsorbents was performed by N_2 adsorption and mercury porosimetry studies. The N_2 adsorption was carried out at 77 K on a Micrometrics ASAP 2420, to determine the Brunauer-Emmett-Teller (BET) surface area, total area, and pore volume [53]. The N_2 isotherms are presented in Fig. 1. As can be observed, the adsorbents reveal type-IV isotherms with a hysteresis loop of the H4 type, based on IUPAC classification [54]. The mercury porosimetry studies were performed on a Micromeritics AutoPore IV 9500, at a pressure of 0.5–33 000 psia to determine the textural properties of the pellets, e.g., density and porosity. The data are summarized in Tab. 2, and the pore size distribution is reported in Sect. S2.

Table 2. Physical properties of BETA zeolites, mercury porosimetry data, and N_2 adsorption data.

Structure type	H-BETA-25	H-BETA-150	Na-BETA-25
Physical characteristics			
Pellet diameter [mm]	3.17	1.59	–
Pellet length [mm]	≈ 2	≈ 4	–
Diameter sieve [mm]	–	–	4.75[a)]–2.00[b)]
Mercury porosimetry data			
Average pore diameter [Å]	242	130	–
Bulk density (at 0.51 psia) [g mL^{-1}]	0.69	1.01	–
Apparent (skeletal) density [g mL^{-1}]	1.40	1.21	–
Porosity [%]	50.59	16.87	–
N_2 adsorption data			
BET surface area [m^{2}g^{-1}]	440.53	516.80	594.39
Total area in pores [m^{2}g^{-1}]	114.23	118.87	131.75
Total volume in pores [cm^{3}g^{-1}]	0.60	0.40	0.48

[a)]Agglomerates used in adsorption studies; [b)]agglomerates used in ZLC studies.

Table 1. Physicochemical properties of the studied adsorbates [62].

Adsorbate	Kinetic diameter [Å]	Dipole moment [×10^{18} esu cm]	Quadrupole moment [×10^{26} esu cm^2]	Polarizability [×10^{26} cm^3]
CO_2	3.30	0.00	4.30	26.50
CH_4	3.80	0.00	0.00	26.00
N_2	3.64	0.00	1.52	17.60

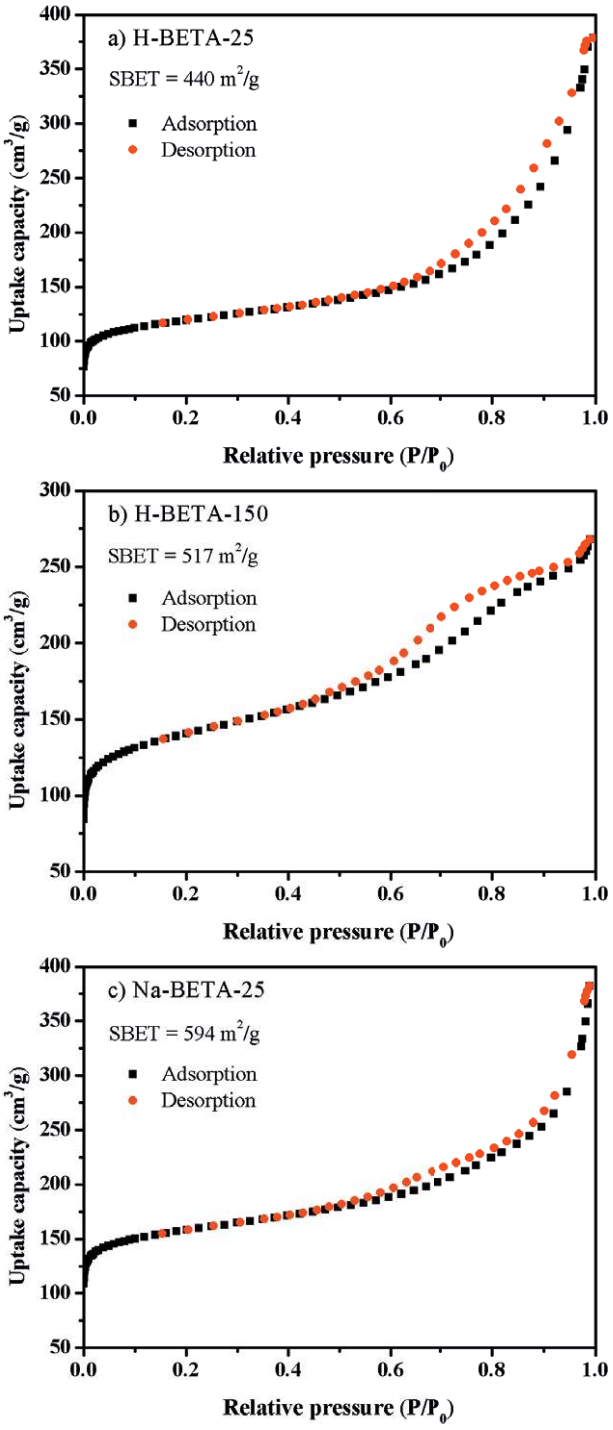

Figure 1. Nitrogen isotherms of adsorption-desorption of (a) H-BETA-25, (b) H-BETA-150, (c) Na-BETA at 77 K.

2.4 Breakthrough Measurements

Studies on fixed-bed adsorption of CO_2, CH_4, and N_2 were performed on a home-made apparatus, as presented in Fig. 2. More details can be found in a previous study [21].

The experimental unit consists of a gas chromatograph, where the adsorption column is placed in an oven equipped with a thermal conductivity detector (TCD). Helium as the carrier gas enters to the system by two different streams. One is mixed with the adsorbate species (CO_2, CH_4, or N_2) to dilute the inlet flow for the column at a fixed partial pressure, and the other one is a pure helium stream employed to desorb the fixed bed. The flow rates are set up by mass flow controllers (MFC). In addition, the pressure of the system is controlled by a back-pressure regulator (BPR). The outlet stream is sent to the TCD, which measures the concentration of all gases.

The experiments involve three main steps: activation of samples, adsorption process, and analysis of data. During the first step, the adsorbent is activated by heating the bed from ambient temperature to 473 K for a period of at least 12 h, under pure helium flow, to remove the impurities and moisture inside the porous adsorbent material. Then, in the second step, a constant flow rate of the mixture (carrier gas and adsorbate) is directed by a three-way valve to the system for the measurement of a typical breakthrough curve at a fixed temperature and partial pressure.

In this work, six different adsorption pressures have been tested at three temperatures for all studied samples. The outlet stream of the bed passes through the TCD. The recorded data is used to set up the breakthrough curve of the experiments. Then, by applying a mass balance on the breakthrough curve, the equilibrium loading is obtained for a specific temperature and partial pressure of adsorbates by the following equation:

$$Q_{\text{adsorbate}} = \frac{1}{m_{\text{adsorbent}}} \left[\int_0^{t_s} \left(F_{\text{gas,in}} - F_{\text{gas,out}}\right) \mathrm{d}t - \frac{y_{\text{gas,feed}} P_b \varepsilon_T V_b}{Z R_g T_b} - \frac{y_{\text{gas,feed}} P_b V_d}{Z R_g T_b} \right] \quad (1)$$

Here, $m_{\text{adsorbent}}$[1)], t_s, $F_{\text{gas,in}}$, $y_{\text{gas,feed}}$, P_b, and V_b are the mass of adsorbent in the bed, saturation time of the bed, molar flow rate of adsorbate at the inlet of the bed, molar fraction of adsorbate in the feed stream, partial pressure, and bed volume, respectively. V_d and T_b represent the dead volume and temperature of the bed at equilibrium condition, respectively. In addition, ε_T is the total porosity of the bed, which is calculated by the following equation [55]:

$$\varepsilon_T = \varepsilon_b + (1 - \varepsilon_b)\varepsilon_p \quad (2)$$

where ε_p is the particle porosity and ε_b is the packed-bed porosity. Finally, the desorption process takes place by switching the gas flow rate to the carrier gas (He) to desorb the adsorbates (CO_2, CH_4, and N_2) from the bed. The employed column for measuring the breakthrough curves had 10 mm internal diameter and 120 mm length and was entirely filled with the adsorbent materials.

1) List of symbols at the end of the paper.

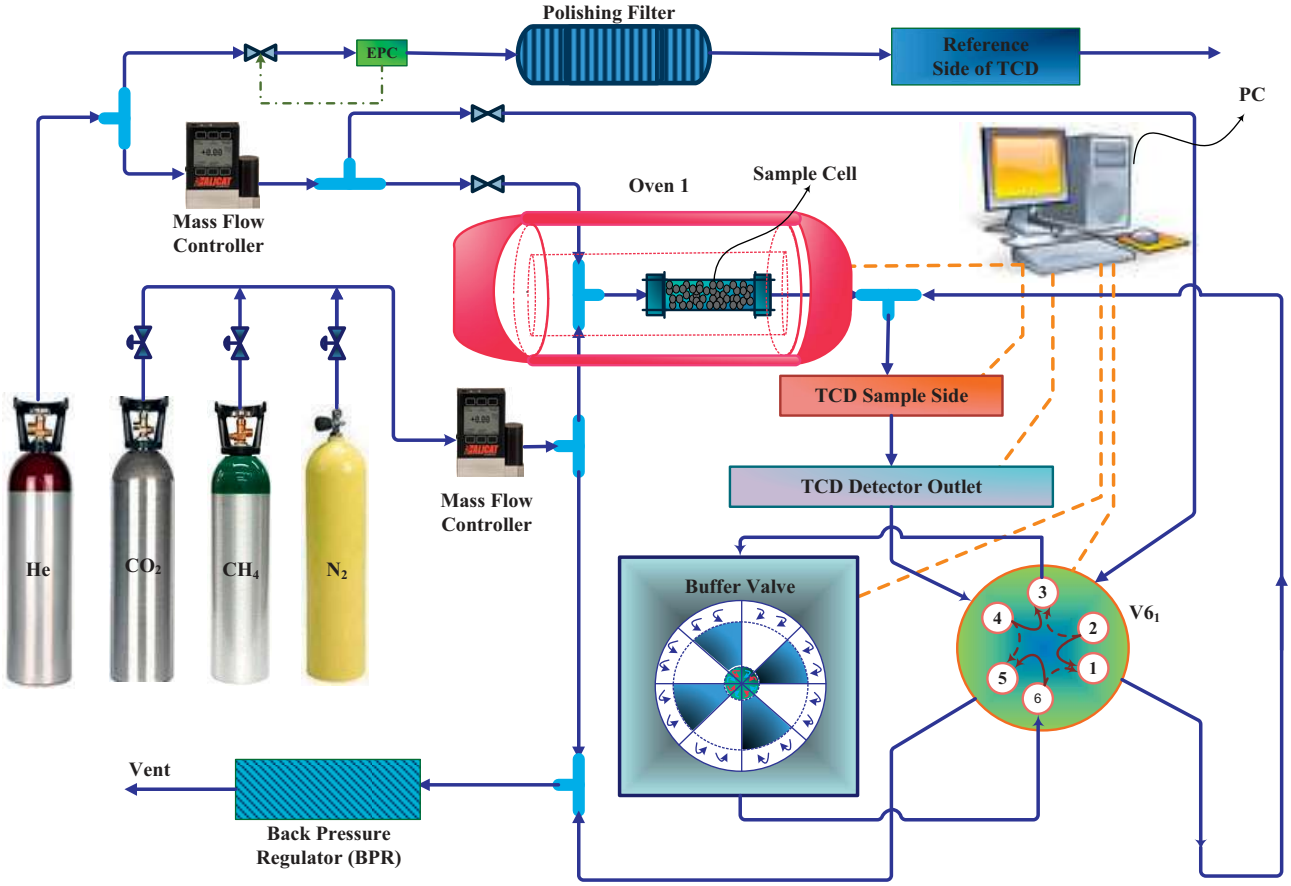

Figure 2. Schematic diagram of the utilized experimental apparatus to measure the adsorption equilibibrium data and ZLC constants.

2.5 ZLC Experiments

The ZLC technique was developed by Eic and Ruthven [56] which is a straightforward technique for measuring intra/extracrystalline diffusivities in porous adsorbents. This technique involves the saturation of a differential bed of porous particles with the sorbate species at a very low concentration under the validity of the Henry's law. Then, the bed is desorbed at a constant flow rate of inert gas. The desorption curve is measured as function of time. This curve indicates important information regarding the diffusion mechanism inside the porous adsorbents and also the kinetic data.

The employed column for ZLC experiments in this work has 4.4 mm internal diameter and 81 mm length, and only the bottom is filled with a small amount of the adsorbent for the ZLC tests.

3 Theory

3.1 Langmuir Model

Among the different available adsorption models, the Langmuir model is the simplest one to fit type-I isotherms [57, 58]. This theoretical model has been derived based on some assumptions including: the adsorption energy of all sites are the same, each site can only hold one adsorbate molecule, there are not any interactions between adsorbed molecules on the neighboring sites, and also there are definite adsorption sites [58]. Thus, in this work, the Langmuir model has been applied to evaluate the obtained equilibrium results. The mathematical formula of this model is as follows [57]:

$$\theta = \frac{q}{q_M} = \frac{bp}{1+bp} \tag{3}$$

where $\theta = q/q_M$ is the degree of filling of sites, q is the adsorbed amount at equilibrium, q_M is the maximum adsorption capacity, b is the adsorption equilibrium constant, and p denotes the partial pressure of components. The b constant indicate the attraction force between the adsorbate molecule onto the surface of the adsorbent, which is calculated by the Van't Hoff equation [58]:

$$b = b_0 e^{\left(\frac{\Delta H}{RT}\right)} \tag{4}$$

where b_0 is the pre-exponential factor of the affinity constant, ΔH is the heat of adsorption, R is the universal gas constant, and T is the experimental temperature. As the adsorption is an exothermic process (ΔH negative), the b constant decreases by

increasing temperature. Henry's law can be obtained from the Langmuir isotherm at a very low partial pressure:

$$q = q_m bp = Hp \tag{5}$$

where H is the Henry constant.

3.2 ZLC Model

The simple form of the ZLC model after applying some assumptions can be presented by a linear equation in a semi-log plot [56]:

$$Ln\left(\frac{C_{out}}{C_0}\right) = Ln\left(\frac{2L}{\beta_1^2 + L(L-1)}\right) - \tau_{dif}\beta_1^2 t \tag{6}$$

where

$$\beta_1 \cot(\beta_1) + L - 1 = 0 \tag{7}$$

C_o is the saturation concentration of the ZLC cell, C_{out} is the outlet concentration of ZLC, t is the time, τ_{dif} is the diffusion time constant, $J_1(\beta_1)$ and $J_0(\beta_1)$ are Bessel functions of first and zero order, and L is a model parameter.

The diffusional time constant (τ_{dif}) and the L parameter depend on the diffusion control mechanism. For systems under micropore diffusion control, τ_{dif} and L are represented by Eqs. (8) and (9), while for macropore diffusion control, these parameters are calculated by Eqs. (10) and (11).

$$\tau_{dif.micropore} = \left(\frac{D_C}{r_C^2}\right)t \tag{8}$$

$$L_{microporo} = \frac{1}{3}\frac{F}{KV_S}\frac{r_C^2}{D_C} \tag{9}$$

$$\tau_{dif.macroporo} = \left(\frac{D_P}{R_P^2(1+K)}\right)t \tag{10}$$

$$L_{macroporo} = \frac{1}{3}\frac{F}{V_S}\frac{R_P^2}{D_P} \tag{11}$$

where D_C is the crystal diffusivity, r_C is the crystal radius, F denotes the flow rate of purge gases, K is Henry's law constant (dimensionless), V_S is the volume of the adsorbent, D_p means the macropore diffusivity and R_p the pellet radius.

Macropore diffusion is generally a combination of Knudsen diffusivity in series with molecular diffusion, so it can be calculated by:

$$D_P = \frac{1}{\Gamma_P\left(\frac{1}{D_m} + \frac{1}{D_K}\right)} \tag{12}$$

where Γ_p is the tortuosity, D_m is the molecular diffusivity, and D_K denotes the Knudsen diffusivity, which is obtained by:

$$D_K = 9700 r_{poro}\left(\frac{T}{M}\right)^{\frac{1}{2}} \tag{13}$$

T is the temperature and M the molecular weight.

However, if the ZLC experiments are performed in the equilibrium regime, the following equation is valid:

$$Ln\left(\frac{C}{C_0}\right) = -\frac{F}{KV_S}t \tag{14}$$

3.3 Response Surface Methodology (RSM)

RSM for statistical analysis of the adsorption process was applied for investigation, analysis, and verification of experimental results as well as determining the interaction effects of the main independent variables. In this process, adsorption temperature (T) and adsorbate partial pressure (P_{com}) have the main influence on the adsorption behavior, thus, they have been chosen as model factors. On the other hand, the adsorption capacity of adsorbents (Q) which is the objective function of the adsorption process, has been considered as model response. To this goal, a polynomial function is applied to the mathematical-statistical treatment of experimental data, and by considering two independent variables, a second-order two independent polynomial function is derived as follows:

$$y = \beta_0 + \beta_1 x_1 + \beta_2 x_2 + \beta_{12} x_1 x_2 + \beta_{11} x_1^2 + \beta_{22} x_2^2 + \varepsilon \tag{15}$$

Here, y is the response value; x_1 and x_2 are the independent variables, which are defined in the range of [0–1] as coded values for model factors; β_0 is the intercept coefficient, β_1 and β_2 represent the linear coefficients of independent variables, and β_{11} and β_{22} display the quadratic coefficients of the main factors. The interaction effect between these variables is expressed by β_{12} and the residual error is considered in the last term ε [59]. The β coefficients of Eq. (15) are calculated by applying the least square method and multiple regression analysis with the lowest possible residual error and it contributes to a general correlation for prognostication of other required values.

In the next step, analysis of variance (ANOVA) and lack-of-fit are applied for statistical evaluation of the model as well as assessment of the fitness of the quadratic model to detect the significance of the regression model for experimental results [60]. In this way, the ANOVA results determine the significant model for statistical analysis of the adsorption process which should have a non-significant lack-of-fit and acceptable p-values. In the last step, the accuracy of the model is evaluated by considering the adjusted coefficient of determination (Adj-R^2) [61].

4 Results and Discussion

4.1 Adsorption Isotherms

As previously mentioned in this work, the adsorption equilibrium isotherms for single components, namely, CO_2, CH_4,and N_2, were measured by a breakthrough technique. Experimental data were collected at different temperatures, 313 K, 373 K, and 423 K, and various partial pressures in the range of 0.33–4.16 bar. The experimental conditions of all performed

runs, including flow rates of adsorbates and helium, partial pressure of adsorbate, and total pressure of the process, which have been the same for all samples, are reported in Tab. 3.

Table 3. Experimental conditions for the breakthrough measurements of CO_2, CH_4, and N_2 on BETA zeolites.

Run	Helium flow rate (NTP)[a)] [mL min^{-1}]	Adsorbate flow rate (NTP)[a)] [mL min^{-1}]	Total pressure [bar]	Adsorbate partial pressure [bar]
1	44.0	22.0	1	0.33
2	14.2	22.0	1	0.61
3	14.2	22.0	2	1.22
4	14.2	22.0	4	2.43
5	14.2	40,0	4.5	3.32
6	8.1	40,0	5.0	4.16

[a)] NTP: normal conditions of temperature and pressure.

The adsorption equilibium isotherms for H-BETA-25, H-BETA-150, and Na-BETA-25 are illustrated in Figs. 3–5, respectively. In these figures, marker points express the experimental data while the solid curves represent the results of the applied isotherm model. As can be seen, the uptake capacity of all zeolite samples increases by enhancing the partial pressure. Also at a fixed partial pressure, when the temperature increases, the adsorption capacity is reduced in accordance with the exothermicity behavior of the adsorption process. For more information, all collected breakthrough curves to set up the isotherms are presented in Sect. S3.

As can be observed in Figs. 3–5, CO_2 has the higher adsorption capacity than CH_4 and N_2 for all adsorbents and studied temperatures and pressures, which can be elucidated based on the lower kinetic diameter [37–39]. Also, CO_2 has a higher quadrupole moment (4.30×10^{-26} esu cm^2) than CH_4 and N_2 which causes a strong attraction of molecules to the electrostatic field of the cationic zeolite sites [62, 63]. At 313 K and 4.16 bar, the adsorbed amounts of CO_2, CH_4, and N_2 are 2.28, 1.31, and 0.83 mol kg^{-1}, respectively, for zeolite H-BETA-25 and 2.23, 1.06, and 0.59 mol kg^{-1} for zeolite H-BETA-150. The values for zeolite Na-BETA-25 are 2.84, 1.59, and 0.97 mol kg^{-1}, respectively. A comparison between the uptake capacities of all studied zeolites for CO_2, CH_4, and N_2 at different pressures and temperatures is depicted in Sects. S4 and S5.

In this work, the isotherms were modeled by a numerical procedure in order to minimize the absolute difference (Δq) between the predicted values (q) by applying the Langmuir model and obtained experimental values (q_{exp}) according to the following equation:

$$\Delta q = \sum_{i=1}^{M} (q - q_{exp}) \tag{16}$$

where M is the total number of experiments. To keep thermodynamic consistency, the q_M parameter is kept constant for three zeolites [64]. Moreover, the q_M value for the Na-BETA-25 zeolite was multiplied by 1.2 because of the binderless nature of the material. Therefore, the fitted value of the saturation capacity of Na-BETA-25 becomes 5.26 instead of 4.39 mol kg^{-1}, which is the same value for H-BETA-25 and H-BETA-150. The Langmuir parameters and the performance of fitting based on correlation coefficients are reported in Tab. 4.

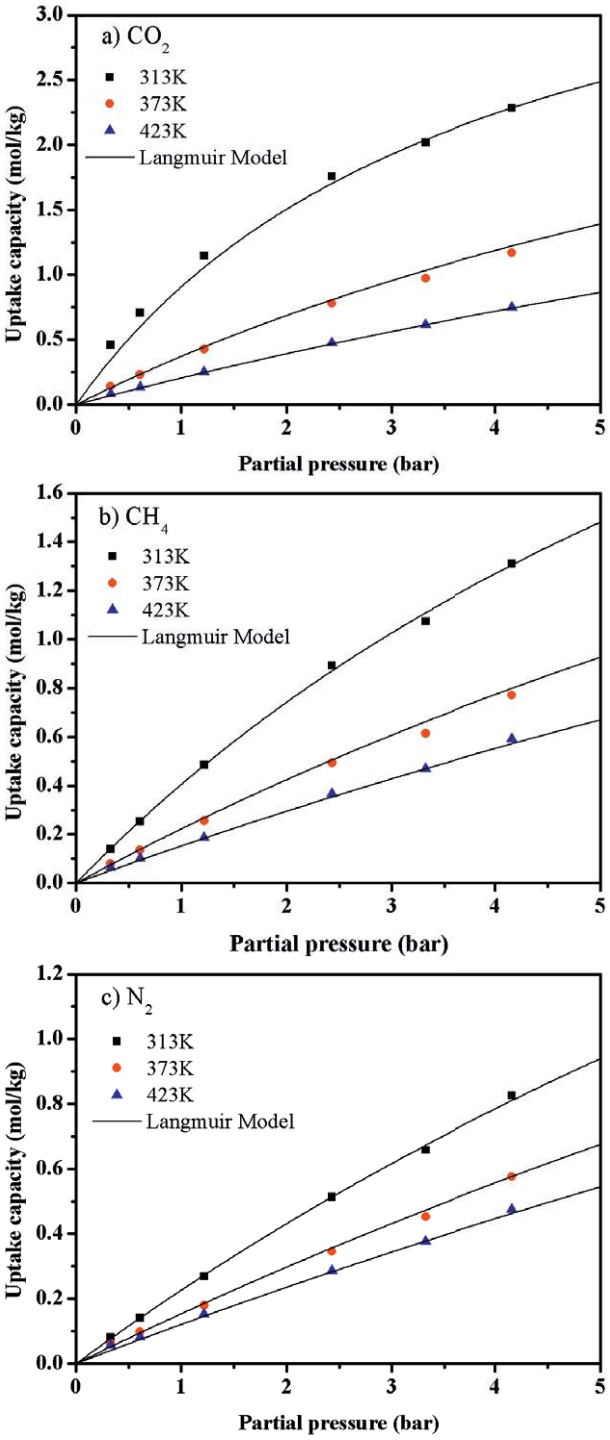

Figure 3. Adsorption equilibium isotherms of (a) CO_2, (b) CH_4, (c) N_2 on the pellets of H-BETA-25 zeolite.

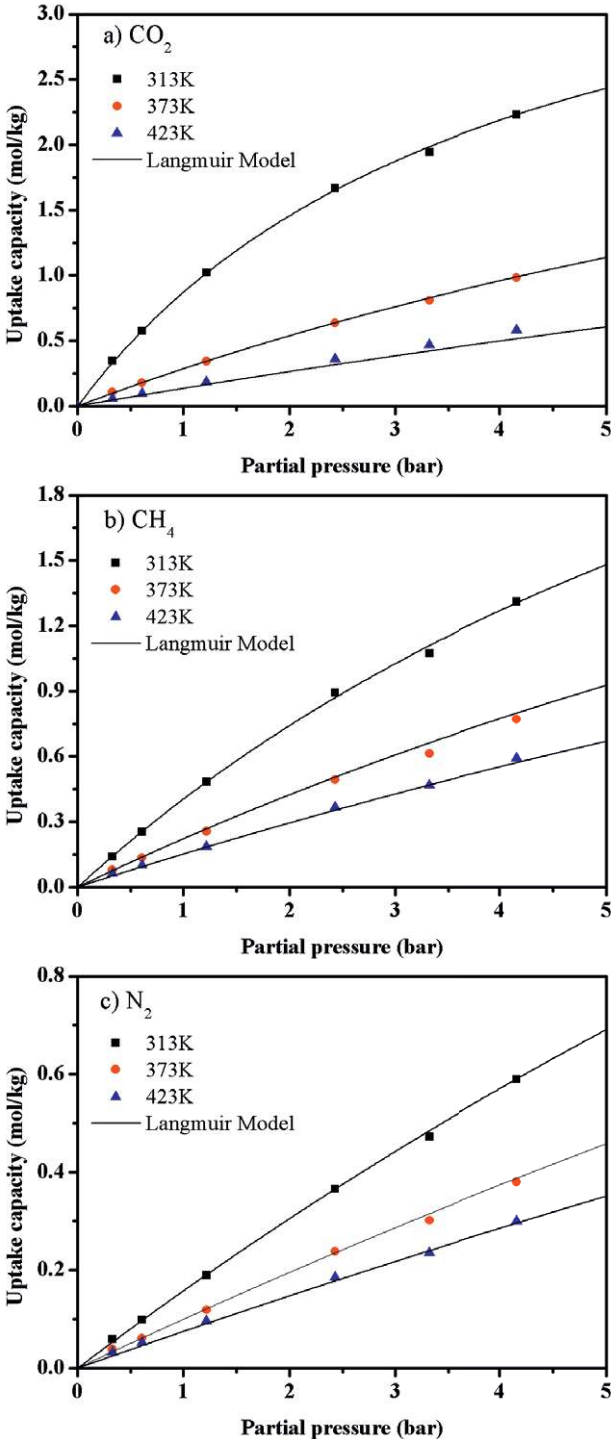

Figure 4. Adsorption equilibium isotherms of (a) CO_2, (b) CH_4, (c) N_2 on the pellets of H-BETA-150 zeolite.

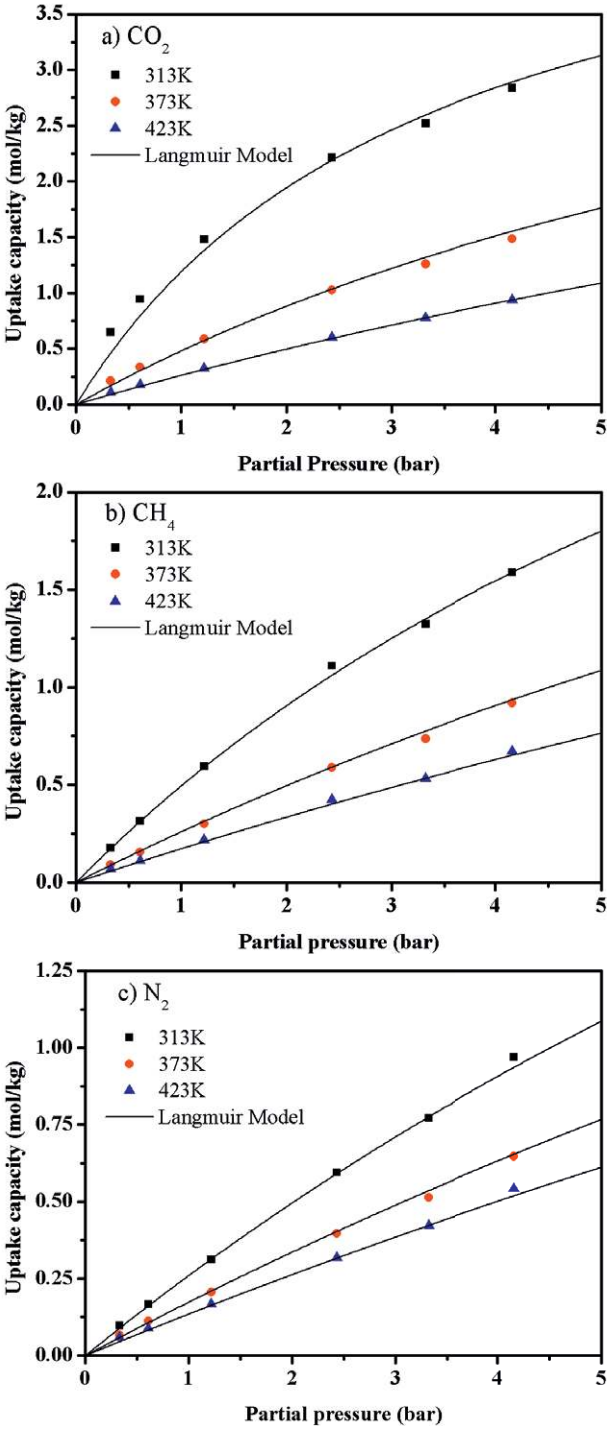

Figure 5. Adsorption equilibium isotherms of (a) CO_2, (b) CH_4, (c) N_2 on agglomerates of Na-BETA-25 zeolite.

The heat of adsorption ($-\Delta H$) also follows the affinity order of the molecules. For adsorbents with the same SiO_2/Al_2O_3 ratio, i.e., 25, the Na^+-containing zeolite shows slightly higher values, with results around 17.3, 11.2, and 6.8 kJ mol^{-1} for CO_2, CH_4, and N_2, respectively.

Validation of the Langmuir isotherm model to represent the equilibrium data of CO_2, CH_4, and N_2 on the studied zeolites can be achieved in a semi-log plot of $\theta/1-\theta/p$ against θ. If the model is valid, the data should evolve parallel to the fractional coverage (axis x) through a linear behavior. The semi-log plots

Table 4. Parameters of the Langmuir model for the adsorption isotherms on BETA zeolites.

	H-BETA-25			H-BETA-150			Na-BETA-25		
	CO_2	CH_4	N_2	CO_2	CH_4	N_2	CO_2	CH_4	N_2
q_{max} [mol kg^{-1}]	4.39	4.39	4.39	4.39	4.39	4.39	5.26	5.26	5.26
$-\Delta H$ [kJ mol^{-1}]	16.76	10.41	6.55	20.53	11.77	7.63	17.31	11.21	6.84
b_0 [bar^{-1}]	4.17×10^{-4}	1.86×10^{-3}	4.39×10^{-3}	9.34×10^{-5}	8.32×10^{-4}	1.97×10^{-3}	3.80×10^{-4}	1.40×10^{-3}	3.77×10^{-3}
Temperature 313 K									
b [bar^{-1}]	0.2606	0.1017	0.0544	0.2482	0.0765	0.0373	0.2928	0.1039	0.0520
H [mol kg^{-1}bar^{-1}]	1.145	0.447	0.239	1.090	0.336	0.164	1.542	0.547	0.274
Temperature 373 K									
b [bar^{-1}]	0.0925	0.0534	0.0363	0.0698	0.0370	0.0233	0.1006	0.0520	0.0341
H [mol kg^{-1}bar^{-1}]	0.407	0.235	0.159	0.307	0.163	0.102	0.529	0.274	0.180
Temperature 423 K									
b [bar^{-1}]	0.0489	0.0359	0.0283	0.0320	0.0236	0.0174	0.0520	0.0339	0.0263
H [mol kg^{-1}bar^{-1}]	0.215	0.158	0.124	0.140	0.104	0.076	0.274	0.179	0.138
$\Sigma\Delta_q$ [mol kg^{-1}]	0.606	0.235	0.139	0.326	0.153	0.088	0.880	0.244	0.160

of H-BETA-150 for CO_2, CH_4, and N_2 are illustrated in Fig. 6. As can be observed, for all gases the experimental data evolve nearly in a horizontal line for the considered range of temperature and partial pressure. Therefore, it can be confirmed that the Langmuir model is able to predict the adsorption equilibrium of CO_2, CH_4, and N_2 gases. Similar results for H-BETA-25 and Na-BETA-25 zeolites are reported in Sect. S6.

Tab. 5 indicates the selectivity for CO_2/CH_4, CO_2/N_2, and CH_4/N_2. The separation factor is constant and it can be calculated in terms of the sorption selectivity S as follows:

$$S\left(\frac{A}{B}\right) = \frac{b_A}{b_B} = \frac{b_0^A\, e^{\left(\frac{-\Delta H_A}{RT}\right)}}{b_0^B\, e^{\left(\frac{-\Delta H_B}{RT}\right)}} \tag{17}$$

where A is the most adsorbed component.

As can be observed in Tab. 5, the selectivity of all studied samples has a descending order, i.e., $CH_4/N_2 < CO_2/CH_4 < CO_2/N_2$, for all three recorded temperatures. Also, the H-BETA-150 zeolite has the highest selectivity among all samples at a temperature of 313 K, with values of 6.65, 3.24, and 2.05. At the same temperature, the H-BETA-25 zeolite showed the lowest selectivity values (4.79, 2.56, and 1.87). By increasing the temperature, the selectivity values decrease and at 423 K, the selectivity for the CH_4/N_2 system is very low, almost close to 1.

The cation exchange from H^+ to Na^+ enhances the adsorption of CO_2 molecules more than in the other two gases. The higher loading of CO_2 can be explained by the strong interaction of CO_2 and the Na^+ in the framework [65]. The Na cation neutralizes the acidity of the zeolite framework by developing the basicity on the structure, which improves the acid adsorption of CO_2. Thus, the Na-BETA zeolite is considered to provide two kinds of adsorption sites for the CO_2 molecules: the strong adsorption on the cationic site and the poor adsorption on its pore wall. Regarding the other two gases, an increase in the adsorbed amount of CH_4 and N_2 molecules contributes to the polarizing power of the cation. The generated force by its electrostatic field has a greater intensity than the obtained electrostatic field by the H cation.

Table 5. Selectivity of gases in the BETA zeolites.

Solids temperature [K]	Selectivity		
	CO_2/CH_4	CO_2/N_2	CH_4/N_2
H-BETA-25			
313	2.56	4.79	1.87
373	1.73	2.55	1.47
423	1.36	1.73	1.27
H-BETA-150			
313	3.24	6.65	2.05
373	1.89	3.00	1.59
423	1.35	1.84	1.36
Na-BETA-25			
313	2.82	5.63	2.00
373	1.93	2.95	1.52
423	1.53	1.98	1.29

By analyzing zeolites with the same compensation H^+ cation, it was found that the parameter b and also the values of Henry's law are higher for the zeolite with lower SiO_2/Al_2O_3

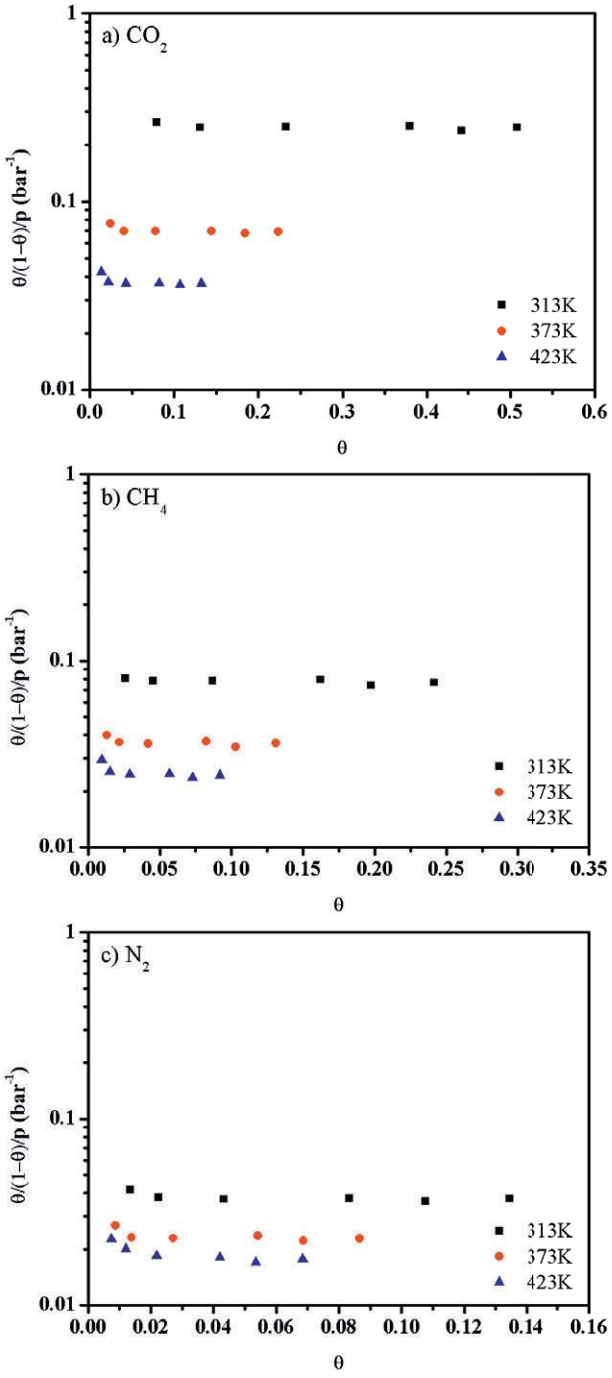

Figure 6. Semi-log plots of $\theta/1-\theta/p$ against θ for analysis of the Langmuir isotherm model for data of (a) CO_2, (b) CH_4, (c) N_2 on H-BETA-150 zeolite.

ratio. A plausible explanation for this effect is based on the amount of compensation cations in the zeolite structure. As the SiO_2/Al_2O_3 ratio increases, the number of cations in the structure is reduced and consequently the intensity of the electrostatically formed fields between the cations and structure declines [66]. This reduction of intensity enhances the hydrophobicity character of the surface and reduces the strong energy polar attraction between the adsorbate molecules onto the surface, and it contributes to the domination of weaker dispersion forces [67]. Thus, CO_2 and N_2 with high and moderate quadrupole moments have adsorbed in a larger amount at lower SiO_2/Al_2O_3 ratios. These results agree well with the ones reported by Stelzer et al. [68], who found that the hydrophobicity index of BETA zeolites increases with higher SiO_2/Al_2O_3 ratio.

With the obtained data for the three BETA zeolites a comparison has been made with other reported adsorbents in Tab. 6. It was observed that in terms of the adsorbed amount of CO_2 under close conditions of temperature and partial pressure the BETA zeolites provided interesting results, mainly for the Na-BETA-25 zeolite. Tab. 6 demonstrates that Na-BETA-25 adsorbs a much higher amount of CO_2 than MIL-101 [69]. It also adsorbed more CO_2 relative to the ZSM-5 [70], β-MEA(40) [38], and close to the value of MOF-508b [63], microwave-activated carbon (MAC), and other β-zeolites, at a slightly lower temperature. The advantage of BETA zeolite over other materials is its ability to alter its hydrophobicity quality [58].

Table 6. Comparison of adsorption capacities of CO_2, CH_4, and N_2 gases on different adsorbents at a partial pressure of ~ 1 bar.

Adsorbent	T [K]	Adsorbed amount [mol kg^{-1}]			Ref.
		CO_2	CH_4	N_2	
MOF-508b	303	1.78	0.64	0.65	[63]
MIL-101	313	0.88	0.14	0.06	[69]
Activated carbon (beads)	303	2.3	1.1	0.3	[71]
Microwave-activated carbon (MAC)	308	1.69	0.81	0.31	[79]
Zeolite 13X (CECA)	308	4.05	0.41	0.20	[72]
Zeolite 13X binderless beads	313	4.4	0.5	–	[25]
ZSM-5	313	1.08	0.65	0.20	[70]
β-Zeolite	303	1.76	0.38	0.14	[37]
β-MEA(40)	303	0.77	0.10	0.03	[38]
β-Zeolite	308	1.82	0.34	–	[39]
STT-zeolite	298	1.42	–	–	[50]
H-BETA-25	313	1.15	0.48	0.27	This work
H-BETA-150	313	1.02	0.38	0.19	This work
Na-BETA-25	313	1.48	0.59	0.31	This work

4.2 Kinetics of Adsorption

The ZLC studies were performed for CO_2 adsorption for all three zeolites, and before preliminary calculations can be made regarding the diffusion mechanism of CO_2 in the BETA zeolite. As the BETA zeolite is considered a large-pore zeolite, it was assumed initially that the mass transfer resistance occurs mainly in the macropores; thus, the performed desorption time of the ZLC experiment in pellets [51], can be estimated by:

$$t = 7\times 10^{-2}\frac{R_P(1+K)}{D_P} \tag{18}$$

where K is the dimensionless Henry's law constant, which is defined as:

$$K = \left(\frac{\rho_P}{\varepsilon_P}\right)H = \left(\frac{\rho_P}{\varepsilon_P}\right)q_M bRT \tag{19}$$

The expected time of the ZLC experiment for the H-BETA-150 zeolite was obtained as around 9 s. In this way, the physical properties of the pellet (Tab. 2) and the adsorption equilibrium parameters (given in Tab. 4) were considered. Also, a value of 0.643 cm^2s^{-1} based on Marrero and Mason [73] for the molecular diffusivity of CO_2-He at 313 K as well as a value of 2 for tortuosity were assumed. For the H-BETA-150 zeolite, the expected time of the ZLC experiment decreased to approximately 5 s. These results proved that the expected time of ZLC experiments is very short and makes it difficult to obtain the kinetic information from the ZLC desorption curves.

Tab. 7 summarizes the ZLC experimental conditions including CO_2 saturation partial pressure, temperature, and purge flow rates with He. Before the experiments, blank runs were performed at flow rates of 30 and 50 mL min^{-1}. The results signified that the cleaning of the ZLC cell occurs very fast.

Table 7. ZLC experimental conditions.

Pressure of the system [bar]	1.00
Partial pressure CO_2 [bar]	0.03
Temperature [K]	313
Purge flow rates (NTP) [mL min^{-1}]	30, 50

Fig. 7 a shows the desorption curves for flow rates of 30 and 50 mL min^{-1} on H-BETA-25. The results for H-BETA-150 and Na-BETA-25 have been reported in Sect. 7. The results for It can be seen from the semi-log plots that the desorption curves are straight lines passing through the horizontal axis, indicating that experiments were performed in an equilibrium regime. Another observed feature in ZLC experiments is the existence of a proportionality between the slope of the desorption curves and value of the purge flow rate. This proportionality is obtained by multiplying the time values of each curve and the respective purge flow rate F; thus, if the curves have an overlap on the semi-log plot, it is a clear indicator for equilibrium regime. This behavior can be observed in Figs. 7 b, S16 b, and S17 b. These results illustrate that the ZLC data is independent

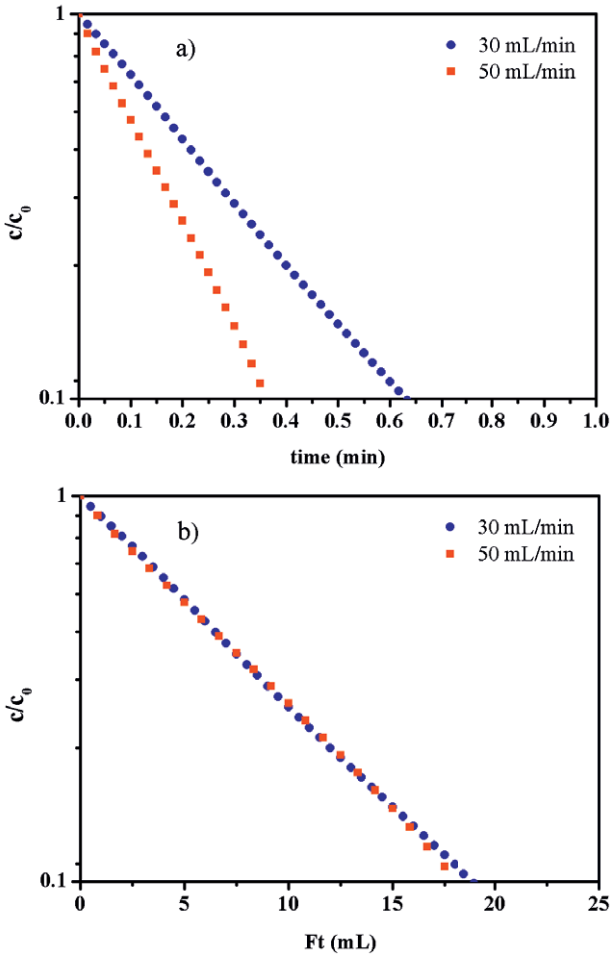

Figure 7. ZLC desorption curves of CO_2 at 313 K on the pellets of H-BETA-25 zeolite. (a) Semi-log plots of C/C_0 vs. time t, (b) semi-log plots of C/C_0 vs. time $\times Ft$.

from D_C/r_C^2 or $D_P/R_P^2(1+K)$, and it is not feasible to obtain any kinetic information from the desorption curves. This also means that the contact time of gas, inside the column (F/KV_S) is much smaller than the diffusional time constant ($D_P/R_P^2(1+K)$) [51].

When the ZLC experiments are in the equilibrium regime, the system is governed by Eq. (14), and the dimensionless Henry's law constant K can be estimated. Then, by using the K values, the ratio of ρ_P/ε_P is calculated by Eq. (19). The estimated values of the experimental slope, dimensionless Henry's constants K, and ρ_P/ε_P ratios are reported in Tab. 8, for all samples. As can be observed, the H-BETA-25 zeolite has the lowest slope compared to the other zeolites with an absolute value of 0.1013 and, consequently, it has the highest Henry's constant with 416.72.

To determine the ρ_P/ε_P relation, according to the physical properties presented in Tab. 2 the value of 5.98 is obtained for the H-BETA-150 zeolite, which is about half of the determined value by the ZLC technique. Some explanations can be given for this anomalous behavior, based on the physical properties of materials. The obtained values for Henry's constant are reli-

Table 8. Parameters estimated by ZLC technique in equilibrium regime.

Adsorbent	–Slope $\ln c/c_0$ [s^{-1}]	Constant K [–]	$\rho_p\varepsilon_p$ [$g\,mL^{-1}$]
H-BETA-25	0.1013	416.72	13.98
H-BETA-150	0.1119	373.13	13.14
Na-BETA-25	0.1124	384.13	9.57

able if there are no errors in the purge flow, also considering that the Langmuir model is fitted well in the experimental measured isotherms. Thus, it can be considered that the obtained difference for the ρ_p/ε_p ratio is related to the values of ρ_p and ε_p which have been determined by the mercury porosimetry technique, or due to the margin of error. However, if the porosimetry values are correct, these results indicate that the measured Henry's constant by the ZLC technique differs by about half of the measured value with the obtained adsorption equilibrium from breakthrough curves.

4.3 RSM Analysis

4.3.1 Adsorption Analysis by RSM

In order to describe the behavior of the adsorption process and also to determine the effects and interactions of the main variables in the process, three RSM models have been developed for CO_2, CH_4, and N_2. The results contributed to the three correlation models which can predict the uptake capacity of CO_2, CH_4, and N_2 on BETA zeolites in the desired operational conditions. To this goal, the experimental results have been fitted with quadratic models to determine the lack-of-fit and statistics situation of the system using multiple regression analysis and the evaluation of the fitness of the model, obtained by ANOVA. In this way, the p-value, standard deviation R^2, predicted determination coefficient (Pred-R^2), adjusted R^2 (Adj-R^2), and lack-of-fit of the initial models should be considered and analyzed to obtain a reliable model.

The obtained results of ANOVA for CO_2 adsorption on Na-BETA-25 as the best sample are presented in Tab. 9. Regression analysis for CH_4 and N_2 are reported in Tabs. S2 and S3, Sect. S8. The results indicate that the models are statistically significant with a p-value < 0.0001, also in all models the lack-of-fit is non-significant, which are the main factors of an authentic model. On the other hand, as can be observed, the R^2, Adj-R^2, and the standard deviation of the RSM models for all components (CO_2, CH_4, and N_2) are acceptable and reliable values. The final models for the studied adsorption process are as follows:

$$Q_{CO_2} = 13.512 - 0.068T + 1.746P_{CO_2} - \left(0.003T \times P_{CO_2}\right) + 0.00008T^2 - 0.0456P_{CO_2}^2 \quad (20)$$

$$Q_{CH_4} = 5.045 - 0.027T + 1.04P_{CH_4} - \left(0.0019TP_{CH_4}\right) + 0.00003T^2 - 0.016P_{CH_4} \quad (21)$$

$$Q_{N_2} = 1.949 - 0.01T + 0.516P_{N_2} - \left(0.0009TP_{N_2}\right) + 0.00004T^2 - 0.001P_{N_2} \quad (22)$$

To describe the behavior of the adsorption process and the effects of the main factors, the obtained coded coefficients should be considered. As can be seen in Tabs. 9, S2, and S3, the linear, the interaction, and the second-order coefficients are significant (p-value < 0.0001) in the proposed model. In addition, the linear coefficients of adsorption temperatures and partial pressures of CO_2, CH_4, and N_2, i.e., (–0.68 and +0.71), (–0.28 and +0.48), and (–0.12 and +0.32), respectively, have significant impacts on the uptake capacities of Na-BETA-25 in comparison with other effects (–0.33, –0.21n and –0.098, respectively, for CO_2, CH_4, and N_2).

Also, the negative linear coefficients of temperatures, i.e., –0.68, –0.28 and, –0.12, respectively, for CO_2, CH_4, and N_2, in a complete accommodation with the Le Chatelier's principle express a negative effect of temperature enhancement on adsorption capacity. The reverse behavior can be inferred to the positive values of linear coefficients of partial pressures.

Table 9. Multiple regression and analysis of variance (ANOVA) of the RSM model for CO_2 adsorption on Na-BETA-25.

CO_2 uptake capacity Q [$mol\,kg^{-1}$]						
	Sum of squares	Mean squares	Coded coefficient	Standard error	df	p-Value
Model	11.11	2.22			5	< 0.0001
T	5.46	5.46	–0.68	0.023	1	< 0.0001
P_{CO_2}	4.88	4.88	0.71	0.025	1	< 0.0001
TP_{CO_2}	0.73	0.73	–0.33	0.031	1	< 0.0001
T^2	0.26	0.26	0.26	0.039	1	< 0.0001
$P_{CO_2}^2$	0.071	0.071	–0.17	0.049	1	0.0052
Residual	0.073	0.006			12	
Total	11.18				17	
Std. dev.	0.078					
R^2	0.9935					
Adj-R^2	0.9907					
Pred-R^2	0.9816					

Based on the values of the interaction coefficients (–0.33, –0.21, and –0.098, respectively, for CO_2, CH_4, and N_2), it can be derived that the pressure increment has a lower effect on the uptake capacity of the process at higher temperatures. The results are listed in Tab. S1. To have a better understanding of the process behavior, 3D plots of the system are depicted in Fig. 8, based on the main factors and response surface for CO_2, CH_4, and N_2 adsorption on Na-BETA-25.

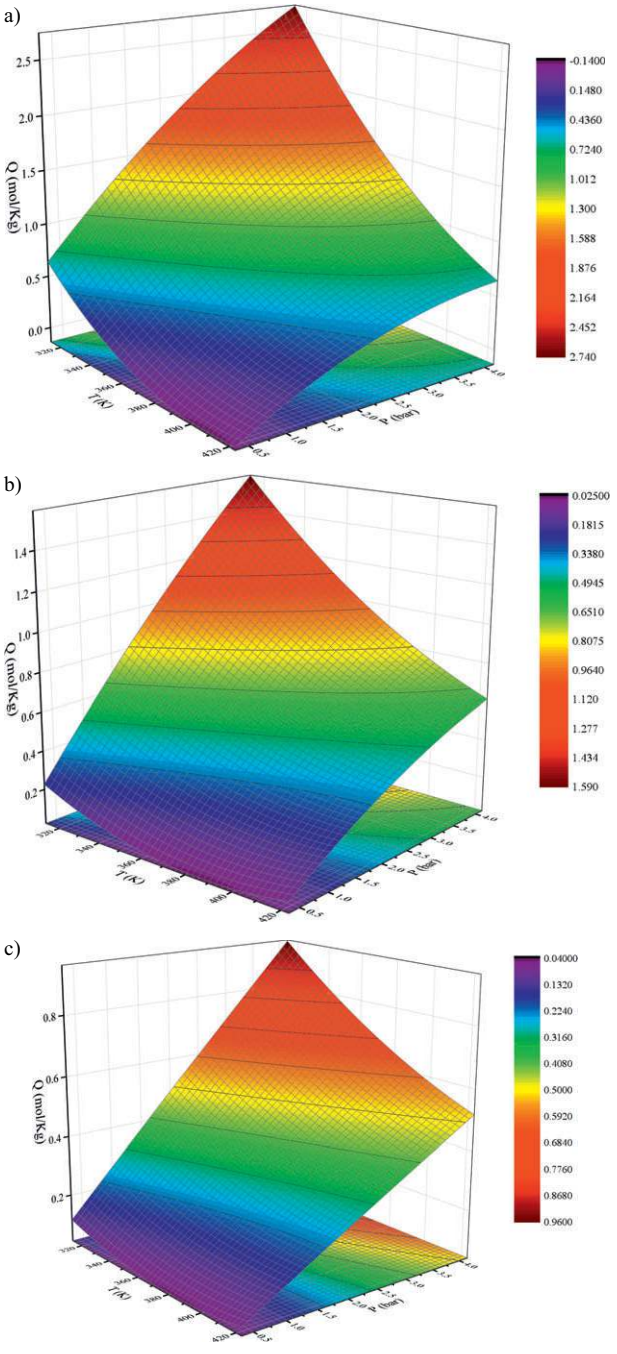

Figure 8. Response surface plots for (a) CO_2, (b) CH_4, (c) N_2 adsorption capacity (mol kg^{-1}) as a function of the independent variables P_p and T.

As can be expected, the enhancement of partial pressure and the reduction of the temperature process increased the uptake capacity of adsorbents, which agrees well with Le Chatelier's principle.

4.3.2 Analysis of the Integrated System by RSM

In the next step, the RSM ability to predict the uptake capacity of zeolites BETA zeolites was considered as an integrated system. In recent years, several studies about intelligent models like artificial neural network (ANN), adaptive neuro fuzzy inference system (ANFIS), and support vector machine (SVM) to predict CO_2 adsorption on activated carbons and amine-solutions were conducted [74–78]. To the best of our knowledge, no study has been published about single-component adsorption by zeolites.

In a similar trend with the previous section, adsorption temperatures and partial pressures of the process were considered as independent variables of the systems (input factors). The uptake capacities of all studied zeolites (H-BETA-25, Na-BETA-25, and H-BETA-150) were determined as a response surface. Then, by using multiple regression analysis and the evaluation of the fitness of the model to a quadratic polynomial, ANOVA was obtained. The results for CO_2 adsorption are reported in Tab. 10 whereas those for CH_4 and N_2 are expressed in Tabs. S4 and S5 in Sect. 8.

Table 10. Analysis of variance (ANOVA) of the proposed model for CO_2 capture on the studied zeolites as an integrated system.

CO_2 capture capacity Q [mol kg^{-1}]						
	Sum of squares	Mean squares	Coded coefficient	Standard error	df	p-Value
Model	25.09	5.02			5	<0.0001
T	12.17	12.17	–0.59	0.030	1	<0.0001
P_{CO_2}	10.93	10.93	0.62	0.033	1	<0.0001
TP_{CO_2}	2.01	2.01	–0.32	0.040	1	<0.0001
T^2	0.69	0.69	0.24	0.052	1	<0.0001
$P^2_{CO_2}$	0.14	0.14	–0.14	0.065	1	0.0417
Residual	1.53	0.032			48	
Pure error	1.34	0.037				
Std. dev.	0.18					
R^2	0.9424					
Adj-R^2	0.9364					
Pred-R^2	0.9247					

As can be found, the proposed RSM model has acceptable values for R^2, Adj-R^2, Pred-R^2, and standard deviation, i.e., 0.942, 0.936, 0.924, and 0.18, respectively. In addition, the obtained model is significant while the lack-of-fit is non-signif-

icant by appropriate p-values (< 0.0001). Thus, the RSM model can propose reliable results for prediction of single-component adsorption by zeolite adsorbents. For more clarification, the CO_2, CH_4, and N_2 uptake capacities on the studied zeolites as an integrated system are depicted in Fig. 9.

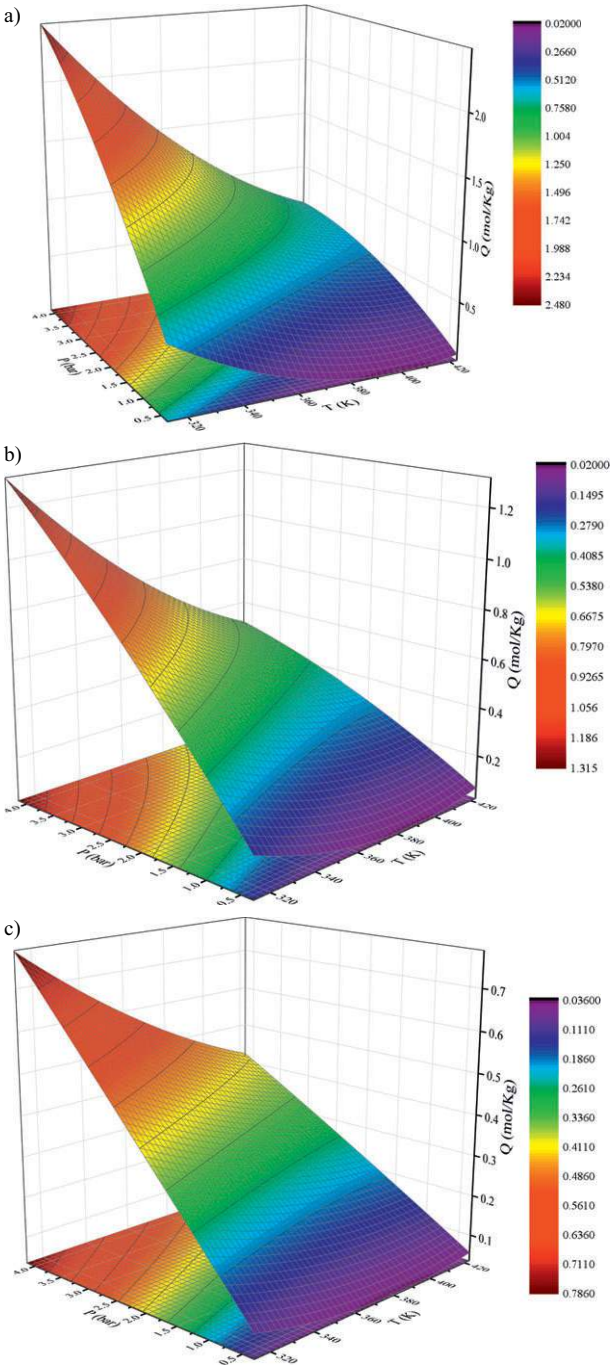

Figure 9. Response surface plots of (a) CO_2, (b) CH_4, (c) N_2 uptake capacity (mol kg^{-1}) on studied zeolites as an integrated system based on the independent variables Pp and T.

5 Conclusions

Three different types of BETA zeolites, namely, H-BETA-25, H-BETA-150, and Na-BETA-25, were tested regarding the adsorption equilibrium for CO_2, CH_4, and N_2 gases. The highest amount of adsorption was experienced for CO_2, followed by CH_4 and N_2. Also, the variations in the BETA zeolite structure, such as the exchange of compensation cations (H^+ by Na^+) and the SiO_2/Al_2O_3 ratio, contributed to the alterations in the adsorption properties. The cation exchange from H^+ to Na^+ enhanced the uptake capacity, mainly for CO_2, and represented the higher selectivity. Changing the SiO_2/Al_2O_3 ratio also brought an important increment in CO_2 adsorption and selectivity.

In addition, it was proved that the determination of the mass transfer mechanism for CO_2, regarding the diffusion studies, by using the ZLC technique is not feasible, but it can be concluded that there are no diffusional resistances under the studied conditions. In sum, it should be noted that the BETA zeolite has interesting characteristics as compared to other materials for treatment of gas mixtures, such as biogas upgrading, especially because its structure can be easily functionalized in terms of cation exchange and hydrophobicity index by the SiO_2/Al_2O_3 ratio. Finally, RSM results point to an excellent ability to model the adsorption process and predict the uptake capacity of zeolites under the required operational conditions.

Acknowledgment

This work was financially supported by the Project POCI-01-0145-FEDER-006984, the Associate Laboratory LSRE-LCM funded by FEDER through COMPETE2020, Programa Operacional Competitividade e Internacionalização (POCI), and by national funds through FCT (Fundação para a Ciência e a Tecnologia). M. Karimi also acknowledges a research grant awarded under project "VALORCOMP" (ref. 0119_VALORCOMP_2_P), financed through INTERREG V A Spain Portugal (POCTEP) 2014–2020, under European Regional Development Fund by FCT. The authors appreciate Süd-Chemie currently acquired by Clariant International Ltd. for kindly providing the samples of BETA zeolites studied in this work.

The authors have declared no conflict of interest.

Symbols used

b	[bar^{-1}]	adsorption equilibrium constant
C_o	[mol m^{-3}]	saturation concentration of ZLC
C_{out}	[mol m^{-3}]	outlet concentration of ZLC
D_c	[$m^2 s^{-1}$]	crystal diffusivity
D_p	[$m^2 s^{-1}$]	macropore diffusivity
D_m	[$cm^2 s^{-1}$]	molecular diffusivity
D_K	[$m^2 s^{-1}$]	Knudsen diffusivity
r_C	[m]	crystal radius
D_{microp}	[mm]	average pore diameter

F	[mL min^{-1}]	flow rate of purge gases
$F_{gas,in}$	[mL min^{-1}]	molar flow rate of adsorbate at the bed inlet
$F_{gas,out}$	[mL min^{-1}]	molar flow rate of adsorbate at the bed outlet
H	[mol kg^{-1}bar^{-1}]	Henry's constant
ΔH	[kJ mol^{-1}]	heat of adsorption
K	[–]	Henry's law constant
M	[g mmol^{-1}]	molecular weight
$m_{adsorbent}$	[g]	mass of adsorbent in the bed
P	[bar]	partial pressure of component
P_b	[bar]	pressure of bed at equilibrium
P_{CH4}	[bar]	partial pressure of methane
P_{CO2}	[bar]	partial pressure of carbon dioxide
P_P	[bar]	partial pressure
P_{N2}	[bar]	partial pressure of nitrogen
q	[mol kg^{-1}]	adsorption capacity at equilibrium condition
q_M	[mol kg^{-1}]	maximum adsorption capacity
R^2	[–]	regression coefficient
R_P	[cm]	pellet radius
S_{BET}	[m^{2}g^{-1}]	specific surface area
S_{ext}	[m^{2}g^{-1}]	external surface area
S_{microp}	[m^{2}g^{-1}]	microporous surface area
t_b	[min]	breakthrough time
t_s	[min]	saturation time
T_b	[K]	temperature of bed at equilibrium
V_b	[cm^3]	bed volume
V_d	[cm^3]	dead volume
V_{microp}	[mm^{3}g^{-1}]	micropore volume
V_S	[m^3]	volume of adsorbent
V_{Total}	[mm^3]	total pore volume
W_{mic}	[nm]	width of micropore
$y_{gas,feed}$	[–]	molar fraction of adsorbate in feed stream
Z	[–]	gas (adsorbate) compressibility factor at P_b and T_b

Greek letters

α	[–]	sticking coefficient
ε	[–]	residual error
ε_b	[–]	packed bed porosity
ε_P	[–]	particle porosity
ε_T	[–]	total porosity of bed
τ_{dif}	[–]	diffusion time constant
Γ_P	[–]	tortuosity

Subscripts and superscripts

Ads.	adsorbent
min	minute
Tot	total

Abbreviations

ANFIS	adaptive neuro fuzzy inference system
ANN	artificial neural network
ANOVA	analysis of variance
RSM	response surface methodology
SVM	support vector machine
ZLC	zero-length column

References

[1] P. Taylor, *Energy Technology Perspectives 2010 – Scenarios and Strategies to 2050 74*, International Energy Agency, Paris **2010**.

[2] P. Nugent, Y. Belmabkhout, S. D. Burd, A. J. Cairns, R. Luebke, K. Forrest, T. Pham, S. Ma, B. Space, L. Wojtas, M. Eddaoudi, M. J. Zaworotko, *Nature* **2013**, *495*, 80–84.

[3] M. Karimi, M. R. Rahimpour, R. Rafiei, M. Jafari, D. Iranshahi, A. Shariati, *J. Nat. Gas Sci. Eng.* **2014**, *17*, 136–150.

[4] A. Khakpay, F. Rahmani, S. Nouranian, P. Scovazzo, *J. Phys. Chem. C* **2017**, *121*, 12308–12320.

[5] M. Karimi, J. A. C. Silva, C. Gonçalves, J. L. Diaz de Tuesta, A. E. Rodrigues, H. T. Gomes, *Ind. Eng. Chem. Res.* **2018**, *57*, 11154–11166.

[6] T. Remy, E. Gobechiya, D. Danaci, S. A. Peter, P. Xiao, L. Van Tendeloo, S. Couck, J. Shang, C. E. A. Kirschhock, R. K. Singh, J. A. Martens, G. V. Baron, P. A. Webley, J. F. M. Denayer, *RSC Adv.* **2014**, *4*, 62511–62524.

[7] M. Ravina, G. J. Genon, *Cleaner Prod.* **2015**, *102*, 115–126.

[8] C. A. Grande, A. E. Rodrigues, *Ind. Eng. Chem. Res.* **2007**, *46*, 7844–7848.

[9] M. Karimi, M. R. Rahimpour, D. Iranshahi, *Chem. Eng. Technol.* **2018**, *41*, 1–14.

[10] J. P. Gutierrez, E. L. A. Ruiz, E. Erdmann, *J. Nat. Gas Sci. Eng.* **2017**, *38*, 187–194.

[11] J. Pires, V. K. Saini, M. L. Pinto, *Environ. Sci. Technol.* **2008**, *42*, 8727–8732.

[12] M. P. S. Santos, C. A. Grande, A. E. Rodrigues, *Ind. Eng. Chem. Res.* **2011**, *50*, 974–985.

[13] M. P. S. Santos, C. A. Grande, A. E. Rodrigues, *Ind. Eng. Chem. Res.* **2013**, *52*, 5445–5454.

[14] D. Georgiou, P. D. Petrolekas, S. Hatzixanthis, A. Aivasidis, *J. Hazard. Mater.* **2007**, *144*, 369–376.

[15] P. H. M. Feron, A. E. Jansen, R. Klaassen, *Energy Convers. Manage.* **1992**, *33*, 421–428.

[16] M. J. Cogbill, G. P. Marsh, *Energy Convers. Manage.* **1992**, *33*, 487–494.

[17] C. Song, *Catal. Today* **2006**, *115*, 2–32.

[18] R. Ben-Mansour, M. A. Habib, O. E. Bamidele, M. Basha, N. A. A. Qasem, A. Peedikakkal, T. Laoui, M. Ali, *Appl. Energy* **2016**, *161*, 225–255.

[19] T. Chronopoulos, Y. Fernandez-Diez, M. M. Maroto-Valer, R. Ocone, D. A. Reay, *Microporous Mesoporous Mater.* **2014**, *197*, 288–290.

[20] Y. Lin, C. Kong, Q. Zhang, L. Chen, *Adv. Energy Mater.* **2017**, *7*, 1601296.

[21] L. Bastin, P. S. Barcia, E. J. Hurtado, J. A. C. Silva, A. E. Rodrigues, B. J. Chen, *Phys. Chem. C* **2008**, *112*, 1575–1581.

[22] R. Sabouni, H. Kazemian, S. Rohani, *Chem. Eng. Technol.* **2012**, *35*, 1085–1092.

[23] R. Sabouni, H. Kazemian, S. Rohani, *Environ. Sci. Technol.* **2013**, *47*, 9372–9380.

[24] J. A. C. Silva, A. F. Cunha, K. Schumann, A. E. Rodrigues, *Microporous Mesoporous Mater.* **2014**, *187*, 100–107.

[25] J. A. C. Silva, K. Schumann, A. E. Rodrigues, *Microporous Mesoporous Mater.* **2012**, *158*, 219–228.
[26] E. Ochoa-Fernández, M. Ronning, T. Grande, D. Chen, *Chem. Mater.* **2006**, *18*, 1383–1385.
[27] S. N. Kim, W. J. Son, J. S. Choi, W. S. Ahn, *Microporous Mesoporous Mater.* **2008**, *115*, 497–503.
[28] *Introduction to Zeolite Molecular Sieves*, 3rd ed. (Eds: J. Cejka, H. van Bekkum, A. Corma, F. Schueth), Elsevier, Oxford **2007**.
[29] B. Smit, T. L. M. Maesen, *Chem. Rev.* **2008**, *108*, 4125–4184.
[30] S. Choi, J. H. Drese, C. W. Jones, *ChemSusChem* **2009**, *2*, 796–854.
[31] International Zeolite Association, *Database of Zeolite Structures*, http://www.iza-structure.org/databases/
[32] R. L. Wadlinger, G. T. Kerr, E. J. Rosinski, *U.S. Patent 3308069*, **1967**.
[33] M. M. J. Treacy, J. M. Newsam, *Nature* **1988**, *332*, 249–251.
[34] A. Corma, L. T. Nemeth, M. Renz, S. Valencia, *Nature* **2001**, *412*, 423–425.
[35] J. D. Lewis, S. van de Vyver, A. J. Crisci, W. R. Gunther, V. K. Michaelis, R. G. Griffin, Y. Roman-Leshkov, *ChemSusChem* **2014**, *7*, 2255–2265.
[36] C. Martinez, A. Corma, *Coord. Chem. Rev.* **2011**, *255*, 1558–1580.
[37] X. Xu, X. Zhao, L. Sun, X. Liu, *J. Nat. Gas Chem.* **2008**, *17*, 391–396.
[38] X. Xu, X. Zhao, L. Sun, X. Liu, *J. Nat. Gas Chem.* **2009**, *18*, 167–172.
[39] Z. Huang, L. Xu, J. H. Li, G. M. Guo, Y. Wang, *J. Chem. Eng. Data* **2010**, *55*, 2123–2127.
[40] J. Stelzer, M. Paulus, M. Hunger, J. Weitkamp, *Microporous Mesoporous Mater.* **1998**, *22*, 1–8.
[41] S. T. Yang, J. Kim, W. S. Ahn, *Microporous Mesoporous Mater.* **2010**, *135*, 90–94.
[42] H. S. You, H. Jin, Y. H. Mo, S. E. Park, *Mater. Lett.* **2013**, *108*, 106–109.
[43] L. Largitte, R. Pasquier, *Chem. Eng. Res. Des.* **2016**, *109*, 495–504.
[44] S. Ghanbari, B. Vaferi, *Mater. Sci Poland* **2017**, *35*, 486–495.
[45] S. Ghanbari, B. Vaferi, *Acta Astronaut.* **2015**, *112*, 19–28.
[46] S. G. Pakdehi, B. Vaferi, *Desalin. Water Treat.* **2016**, *57*, 18286–18292.
[47] H. Maghsoudi, *Adsorption* **2015**, *21*, 547–556.
[48] F. Karamouz, H. Maghsoudi, R. Yegani, *Chem. Eng. Technol.* **2018**, *41*, 1767–1775.
[49] M. J. Vaezi, A. A. Babaluo, H. Maghsoudi, *J. Nat. Gas Sci. Eng.* **2018**, *52*, 423–431.
[50] H. Maghsoudi, A. Aidani, *Adsorption* **2017**, *23*, 963–969.
[51] J. A. C. Silva, A. E. Rodrigues, *Chem. Eng. Technol.* **2015**, *38*, 2335–2339.
[52] *Diffusion in Nanoporous Materials* (Eds: J. Kaerger, D. M. Ruthven, D. Theodorou), John Wiley & Sons, New York **2012**.
[53] S. Brunauer, P. H. Emmett, E. Teller, *J. Am. Chem. Soc.* **1938**, *60*, 309–319.
[54] M. Thommes, K. Kaneko, A. V. Neimark, J. P. Olivier, F. Rodriguez-Reinoso, J. Rouquerol, K. S. W. Sing, *Pure Appl. Chem.* **2015**, *87*, 1051–1069.
[55] J. M. Becnel, C. E. Holland, J. McIntyre, M. A. Matthews, J. A. Ritter, *American Society for Engineering Education Annual Conference & Exposition*, Montréal, Quebec, Canada, **2002**.
[56] M. Eic, D. M. Ruthven, *Zeolites* **1988**, *8*, 40–45.
[57] I. Langmuir, *J. Am. Chem. Soc.* **1916**, *38*, 2221–2295.
[58] D. M. Ruthven, *Principles of Adsorption and Adsorption Processes*, John Wiley & Sons, New York **1984**.
[59] A. Wahby, J. Ramos-Fernandez, M. Martinez-Escandell, A. Sepulveda-Escribano, J. Silvestre-Albero, F. Rodriguez-Reinoso, *ChemSusChem* **2010**, *3*, 974–981.
[60] S. García, M. V. Gil, J. J. Pis, F. Rubiera, C. Pevida, *Int. J. Greenhouse Gas Control* **2013**, *12*, 35–43.
[61] D. Bas, I. H. Boyaci, *J. Food Eng.* **2007**, *78*, 836–845.
[62] T. C. Golden, S. Sircar, *J. Colloid Interface Sci.* **1994**, *162*, 182–188.
[63] P. S. Bárcia, L. Bastin, E. J. Hurtado, J. A. C. Silva, A. E. Rodrigues, B. L. Chen, *Sep. Sci. Technol.* **2008**, *43*, 3494–3521.
[64] R. T. Yang, *Gas Separation by Adsorption Processes*, Butterworth, Boston **1987**.
[65] S. K. Wirawan, D. Creaser, *Microporous Mesoporous Mater.* **2006**, *91*, 196–205.
[66] T. Kawai, K. Tsutsumi, *Colloid Polym. Sci.* **1992**, *270*, 711–715.
[67] M. Sakuth, J. Meyer, J. Gmehling, *Chem. Eng. Process.* **1998**, *37*, 267–277.
[68] J. Stelzer, M. Paulus, M. Hunger, J. Weitkamp, *Microporous Mesoporous Mater.* **1998**, *22*, 1–8.
[69] Y. Zhang, W. Su, Y. Sun, J. Liu, X. Liu, X. Wang, *J. Chem. Eng. Data* **2015**, *60*, 2951–2957.
[70] P. J. E. Harlick, F. H. Tezel, *Sep. Purif. Technol.* **2003**, *33*, 199–210.
[71] Y. J. Wu, Y. Yang, X. M. Kong, P. Li, J. G. Yu, A. M. Ribeiro, A. E. Rodrigues, *J. Chem. Eng. Data* **2015**, *60*, 2684–2693.
[72] S. Cavenati, C. A. Grande, A. E. Rodrigues, *J. Chem. Eng. Data* **2004**, *49*, 1095–1101.
[73] T. R. Marrero, E. A. Mason, *J. Phys. Chem. Ref. Data* **1972**, *1*, 3. DOI: https://doi.org/10.1063/1.3253094
[74] Q. Zhou, Y. Wu, C. W. Chan, P. Tontiwachwuthikul, *Eng. Appl. Artif. Intell.* **2011**, *24*, 673–685.
[75] Q. Zhou, C. W. Chan, P. Tontiwachwuthikul, *Fuzzy Sets Syst.* **2010**, *161*, 2597–2611.
[76] C. Nwaoha, K. Odoh, E. Ikpatt, R. Orji, R. Idem, *J. Environ. Chem. Eng.* **2017**, *5*, 5588–5598.
[77] H. Saghafi, M. M. Ghiasi, A. H. Mohammadi, *Int. J. Greenhouse Gas Control* **2017**, *62*, 23–30.
[78] S. K. Jha, J. Bilalovic, A. Jha, N. Patel, H. Zhang, *Renewable Sustainable Energy Rev.* **2017**, *77*, 297–317.
[79] H. Yi, F. Li, P. Ning, X. Tang, J. Peng, Y. Li, H. Deng, *Chem. Eng. J.* **2013**, *215/216*, 635–642.

